

DNA-polymer architecture orchestrates the segregation and spatio-temporal organization of *E. coli* chromosomes during replication in slow growth conditions.

Debarshi Mitra, Shreerang Pande & Apratim Chatterji*

Dept of Physics, IISER-Pune, Pune, India-411008.

(Dated: October 12, 2021)

The mechanism and driving forces of chromosome segregation in the bacterial cell cycle of *E. coli* is one of the least understood events in its life cycle. Using principles of entropic repulsion between polymer loops confined in a cylinder, we use Monte carlo simulations to show that the segregation dynamics is spontaneously enhanced by the adoption of a certain DNA-polymer architecture as replication progresses. Secondly, the chosen polymer-topology ensures its self-organization along the cell axis while segregation is in progress, such that various chromosomal loci get spatially localized. The time evolution of loci positions quantitatively match the corresponding experimentally reported results, including observation of the cohesion time and the ter-transition. Additionally, the contact map generated using our bead-spring model reproduces the four macro-domains of the experimental Hi-C maps. Lastly, the proposed mechanism reproduces the observed universal dynamics as the sister loci separate during segregation. It was already hypothesized and expected that SMC proteins, e.g. MukBEF contribute over and above entropic repulsion between bacterial-DNA ring-polymers to aid the segregation of daughter DNAs in the *E.coli* cell cycle. We propose that cross-links (plausibly induced by SMC proteins) at crucial positions along the contour is enough to provide sufficient forces for segregation within reasonable time scales. A mapping between Monte Carlo diffusive dynamics time scales and real time units helps us use experimentally relevant numbers for our modeling.

Significance Statement: *The mechanism governing the separation of two sister chromosomes into two halves of the cell before cell division is known for higher organisms, but not yet fully understood for bacterial cells which are much simpler organisms. For E.coli bacterial cells, it is established that certain chromosomal segments get localized along the cell long-axis while replication is in progress. Our simulations establish that a specific looped architecture for the replicating chromosomes provides sufficient entropy driven repulsive forces between loops leading to localization of chromosomal segments and their segregation within observed time scales. Our proposed framework reconciles many spatio-temporal organizational aspects of E. coli chromosome as seen in-vivo and provides a consistent mechanistic understanding of the process underlying segregation.*

The replication and segregation of chromosomes into two halves of the cell before the start of cell division is an important step to maintain the life cycle of a living cell [1, 2]. Nature has devised advanced strategies to segregate the chromosomes of eukaryotes, but interestingly, the mechanism of chromosome segregation of a much simpler single-celled bacterial organism such as the *E. coli* is unknown till date [3–8]. Investigators have identified mechanisms with contributions from proteins which leads to the chromosomal segregation in bacteria *B. subtilis* [8, 9] and *C. crescentus* [8, 10, 11], but any such mechanism could not be identified for *E. coli*.

The chromosome of *E. coli* can be thought of as having ring polymer architecture, and it has been proposed

that the physical principles related to entropy maximization (or equivalently free energy minimization) might be used by nature to achieve chromosome segregation while replication is in progress. It has been shown that entropic repulsion between 2 ring polymers confined within a cylinder lead to their gradual segregation [12–18]. But then it has to be aided by some other hitherto unknown processes driven by proteins, as entropic repulsion is too weak [8] to have segregation within time scale of 60 minutes of the C+D-period [19–21]. This has spawned a series of experiments over the last two decades.

Detailed in-vivo experiments, with DNA-loci labelled with fluorescent markers, have helped us visualize their spatial dynamics as the *E. coli* DNA replicates and simultaneously segregates. The DNA-organization transitions from the ori-ori-ter configuration to the ori-ter-ori configuration in the midst of segregation [22, 23]. As replication proceeds, the rod shaped cell elongates along its long-axis to double its length before cell division occurs. Furthermore, for slow growth conditions (SGC) there is a cohesion time of around 15 minutes (post replication), before the two *oriCs* branch out from the center of the cell and get localized at the two quarter positions along the cell long axis [23]. The variation of *oriC*-position, as measured by the standard deviation of its mean position, is less than one tenth of the length of the cell. Upto 7 other loci are found to be well localized at certain positions along the cell long-axis [23]. In fast growth conditions, with multi-fork replication, the *oriCs* are found in positions $(1/8, 3/8)$, $(5/8, 7/8)$ position along the cell long axis. Though the mechanism of the localization of the *oriC* and other loci remain unexplained, researchers have observed the increase in MukBEF at these positions during segregation. It has been suggested that the positions of the *oriCs* are correlated with the increase of Muk

* Correspondence email address: apratim@iiserpune.ac.in

BEF concentrations [24]. Other dynamical aspects of the segregation process remain unexplained (or controversial) as well, e.g., (i) the sequential start of segregation of the different loci along the chain contour from the cell center (and if that is consistent with the train-track model or the replication factory model) and (ii) the origin of the universal values of drift velocity ($0.33\mu/s$) of loci at the onset of segregation, observed for 8 pairs of genetic loci located on the two daughter chromosomes, respectively [23]. The daughter chromosomes remain conjoined at the *dif* position in the *ter* domain near the cell center till the end of replication, and move apart thereafter.

The experiments, which mark the spatio-temporal distribution of the DNA molecule in individual cells during the segregation process, however lack sufficient resolution. One typically follows just 8 – 13 loci on the DNA molecule. Complementary experiments, which provide more detailed global organization of the DNA-polymer by 5C and Hi-C contact maps [25–28], lose out on the temporal information. These show the existence of topologically associated domains (TADs) and point to the existence of 4 macro-domains in the DNA-organization in the *E. coli* cell [29–32]. The positional correlations presented in Hi-C maps is from data collected from a population of many *E. coli* cells which are at different stages of the cell cycle. Since the replication and segregation constitute of 80% of the cell cycle, any model of segregation should also be consistent with data presented in Hi-C maps. Researchers have several theoretical models (e.g. the loop extrusion and the SBS model) to study the organisation and segregation of chromosomes, both eukaryotic and prokaryotic, which are optimised to obtain a match with the experimental Hi-C map [33–40]. Consensus has not been reached about the origin of the four macro-domains in *E. coli*, though SMC proteins are expected to play a important role [32, 36, 41].

Many studies using coarse-grained polymer models have primarily focused on the organization of chromosome in bacterial or eukaryotic cells [42–53] but relatively fewer on the segregation dynamics of chromosomal loci while replication is in progress [24, 54, 55]. A more detailed framework which reconciles complementary experimental results pertaining to both the spatial and temporal organization of bacterial chromosomes during its life cycle in slow [23] and fast growth conditions [22], incorporating the reported effects of SMC proteins in vivo, is in order [56]. This work aspires to propose an unifying framework addressing these concerns for a replicating chromosome in slow growth conditions.

Our proposed model relies on the concepts of enhanced entropic repulsion provided by the presence of loops within each of the two daughter DNA-polymers. These are created by two additional contacts/links which bridge distant chromosomal regions: cross-links (CLs) created between specific pair of points along the chain contour in the polymer physics terminology. Thereby, we propose that the daughter DNAs adopt a slightly more evolved architecture than just a simple ring polymer, as replica-

tion proceeds. This simple but pivotal idea provides a consistent picture of the segregation of *E. coli* daughter DNAs after replication, and quantitatively integrates disparate experimental measurements on (a) localization of loci along cell long-axis, (b) observation of four macro-domains in Hi-C maps, (c) universal speeds of loci at the onset of segregation before reaching their home positions and (d) enhanced propensity to segregate resulting in lower segregation time scales of daughter DNAs as replication proceeds.

Nucleoid associated proteins (NAPs) play an important role in *E. coli* segregation [14, 32]. They compactify the bacterial DNA at all length scales and also help bridge distant chromosomal segments. It has been shown previously that depletion of some SMC proteins like MukBEF leads to defects in the segregation of the *E. coli* chromosome, thus underlining their importance [25, 32, 57]. We propose that the role of SMCs (and MukBEF in particular) is to facilitate the segregation of replicating chromosomes by modifying their loop architecture suitably, such that they are more amenable to segregation by entropic means. We identify particular architectures, which increase segregation speeds significantly to bring down the segregation time.

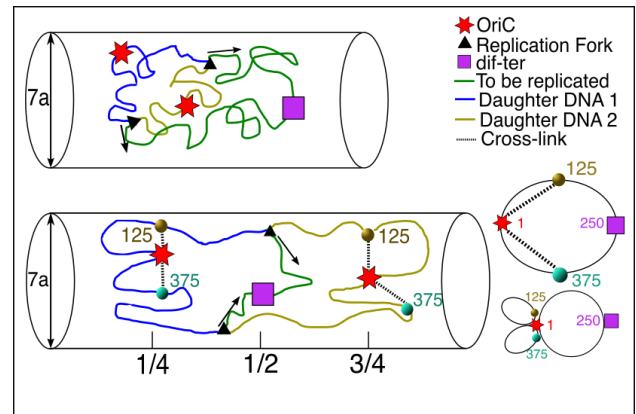


FIG. 1. The upper cylinder shows the *ori-ori-ter* DNA-polymer configuration at the start of replication. The configuration spontaneously evolves to the *ori-ter-ori* configuration, as seen in the lower cylinder, as replication progresses. The cylinder elongates as replication proceeds, and the bottom-cylinder shows the modified Arc-2 polymer architecture in the presence of the 2 cross-links at specific sites for each of the two daughter strands.

The unreplicated DNA of *E. coli* having 4.6 million bp (base pairs), is represented as a bead-spring ring polymer with 500 beads, modified with additional CLs. Thus each bead represents around 9200 bp. It is known that there are topologically distinct domains of size $\sim 10kbp$ in *E. coli* due to gene expression [32, 58]. We also expect contributions from various histone-like HU-proteins (and other NAPs) to compactify the DNA at smaller (10 – 50 nm) length scales. But we expect, that the two cross-links at specific sites considered for this study

to be long-lived, while the rest get on to the backbone or fall off at different times to complete other biological functions, during the life cycle of the cell. These specific CLs bridge segments which are at a distance about $\sim 1\text{Mbp}$ away from each other to create the Arc-2 architecture. The CLs may arise due to MukBEF-activity which are known to create contacts between segments separated by $\sim 900\text{kbp}$ [32, 59]. Two additional CLs at specific sites in the *ter*-macrodomain bridge segments which are $\sim 600\text{kbp}$ apart; we name this as the Arc-2-2 architecture. Thus the CLs are chosen such that the segments in the *ter* macrodomain, are linked to relatively closer segments. Our choice of specific sites for CLs in both Arc-2 and Arc-2-2 was found to be consistent with the recently reported observation that MukBEF activity is hindered in the *ter*-macrodomain due to the presence of MatP [32], which possibly leads to the formation of smaller loops in the *ter*-macrodomain. The choice of the specific cross-linking sites reported here have been chosen from a pool of several other possible polymer-loop architectures having different CL-sites. We use insights gained from our other studies (to be reported elsewhere) to choose Arc-2 and Arc-2-2 architectures due its higher degree of success in reconciling the experimental results.

Model We perform Monte Carlo simulations starting with a polymer of Arc-2 or Arc-2-2 architecture. The unit of length in our simulations is a , which is the equilibrium length of springs between adjacent monomers along chain contour. Each monomer is of diameter $\sigma = 0.8a$ and excluded volume interactions are implemented by the WCA potential. The first monomer in the ring is labelled as the *oriC* and monomer number 250 is assumed to be the *dif*-locus in *ter* domain, hereafter referred to as *dif-ter*. If we chose $a \sim 150\text{ nm}$, which we justify to be a reasonable length scale for 9200 base pairs considering DNA-compaction at smaller length scales, then we can establish that 25×10^3 Monte Carlo steps (MCS) corresponds to 1 second(s) of real time: refer SI-1 and Fig.S1 in the Supplementary Information.

The complex machinery of opening of the mother chromosomal strands by helicase and creating a daughter double stranded DNA is significantly simplified in our model. We model replication explicitly by adding two monomers (9200bp each) at a time to create another chain, unless stated otherwise. The position of two replication forks (RFs) is assumed to start moving bidirectionally from one monomer to the next starting from the *oriC* towards *dif-ter*, as a monomer is added at each RF every 2×10^5 MCS ($\approx 8\text{s}$). This ensures the correct replication rates; also refer SI-II and Fig.S2 for details. After the RF position moves ahead to the next bead, we label the the newly created monomers as those belonging to daughter DNA-2, while the original strand from *oriC* to the RF position is labelled daughter DNA-1. To mimic the effect of topoisomerase which allows release of topological constraints by facilitating chain crossing, we reduce the σ to $\sigma' = 0.1a$ at regular intervals for nearly 8% of the total evolved time: refer SI-II.

We introduce cross-links (CLs) between monomer 1 and 125 immediately after 125-th monomer is replicated. Simultaneously, we also cross-link monomer 1 to 375. Note that the 375-th monomer gets replicated at the same time as the 125-th monomer, refer Fig.1. These additional CLs introduced in both the daughter DNA-polymer are realised by harmonic springs of length a . We call this the Arc-2 architecture. The introduction of the CLs leads to the subsequent movement of the monomer pairs towards each other, unless prevented by topological constraints, which can be released subsequently.

At time $t = 0$, a Arc-2 unreplicated DNA-polymer is confined within a cylinder of diameter $D_c = 7a$ ($\approx 1\mu$) and length $L_i = 17.5a$, with an aspect ratio of 1 : 2.5 and a colloidal volume fraction of 0.2, as is seen in-vivo. As the the DNA gets replicated, the length of the cylinder doubles itself to be $L_f = 35a$, through an incremental increase every 2×10^5 MCS. We perform 150 million MCS in one run, which corresponds to ~ 100 minutes. We do not model the cell division process in our minimal model, which occurs at ≈ 60 minutes in-vivo. Instead, after the completion of replication, the two model daughter chromosomes remain attached at *dif-ter* loci. We follow the positions of different loci of the daughter chromosomes, viz, monomers indexed as 22, 141, 443, 369, 304 and 228 in our ring polymer from the time of replication of these monomers. These position of these monomers along the contour correspond to loci labelled as L1, L2, R1, R2, R3 and *ter1* in [23].

Result : In Fig.2a, we show a representative snapshot of our simulations at the end of replication, with two daughter DNAs where we can identify the positions of the two *oriC* (red circles) and *dif-ter* (blue circle). The color gradient indicates the monomer index of a particular monomer, and the color code is identical for the two DNA-polymers. Thus the reader can see the positional organization of the two polymers as one moves from monomer-1 to 500 along chain contour. Monomers 125 and 375 are close to the *oriC* due to the presence of CLs. In Fig.2b, the data shows the distance between the center of mass (D_{com}) of the two daughter DNA-polymers for 4 independent runs. We see that segregation is typically complete in $\approx 6 \times 10^7$ iterations. We intentionally also show data for run4, to emphasize the infrequent cases where segregation remains incomplete.

In Fig.2c, we also compare entropic segregation of two overlapping ring-polymers without loops (Arc-0 architecture) and the polymer architecture with 2 additional loops (Arc-2). When D_{com} exceeds $11a$ ($\approx 1.5D_c$) and that condition is maintained for the next 4×10^7 MCS we deem the daughter chromosomes to have been segregated. We observe faster segregation in 50 million MCS ($\approx 33\text{ mins}$) with Arc-2, refer Fig.2(c) and SI-III for other details of calculation. The mechanism of segregation is purely entropic. If the two DNA-polymers occupy different halves of the cylinder they can explore more phase space conformations, and therefore segregate [13]. Note that when the daughter chromosomes are *completely seg-*

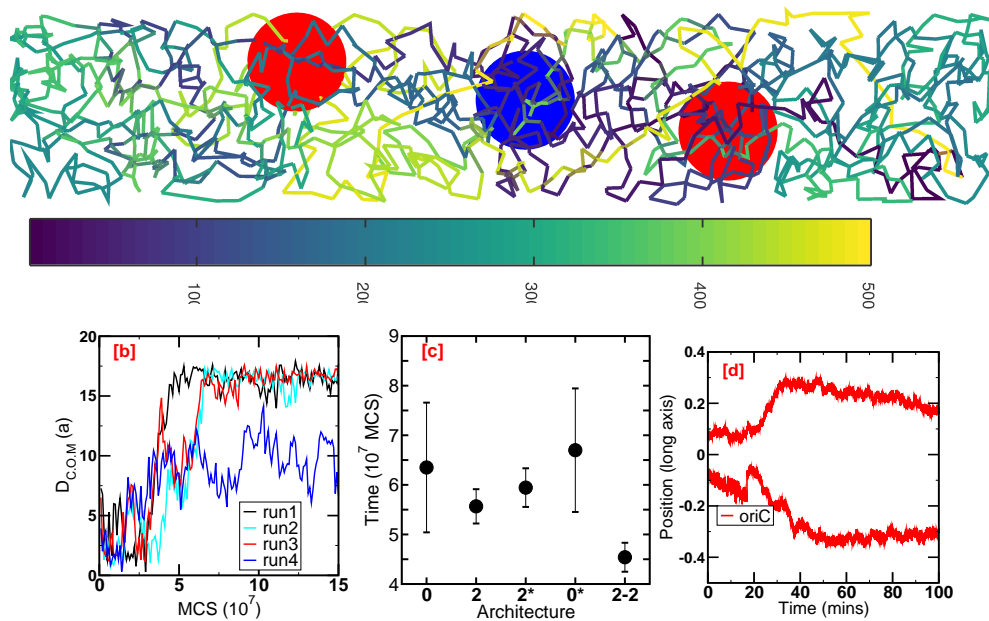


FIG. 2. (a) A representative snapshot of the segregated polymers from our simulation at the end of the replication process at 5×10^7 MCS (equivalently 33.3 mins) is shown. The length of the cylinder (not shown) is $35a$, diameter remains $7a$ ($a \equiv 150\text{nm}$). The two red circles represent the *oriC* at the two quarter positions and the blue circle is the *dif-ter* locus. The colour changes as we move along the contour from monomer 1 to 500: refer colour bar. (b) The distance D_{COM} between the two centers of mass (COM) of each daughter DNA is plotted versus MCS, from the start of replication process. We continue till 15×10^7 MCS, though we expect cell division (not modelled) to occur after 9×10^7 MCS. Data for 4 independent runs (\equiv cell cycles for 4 individual cells) are shown. (c) The segregation time calculated for different architectures (refer main text) is shown. The segregation times have been computed by averaging over 10 independent runs for each architecture. (d) The position of the 2 *oriC*s are shown as a function of MCS, averaged over 20 independent runs. The cylinder doubles its length from $L_i = 17.5a$ to $L_f = 35a$ by 5×10^7 MCS, and the *oriC* positions shown are normalized by L_f . One can map 25 kMCS to 1s: refer SI-1, or equivalently 10^7 MCS \equiv 6mins and 40s.

regated once $D_{com} \approx L_f/2 \equiv 17a$, which might take a bit longer. We avoid this criteria for identifying segregation, because fluctuations in D_{COM} does not maintain $D_{COM} > 17a$ for 4×10^7 MCS.

Moreover, if we introduce the CLs after the replication is complete, referred as Arc-2* in Fig.2c, then the (mean) time τ_S for segregation increases. When chain crossing is not allowed for a simple ring polymer architecture (Arc-0*) they often get entangled and can only segregate in 40% of the attempts. When topoisomerase effects are included by allowing chain cross as for Arc2, Arc2* and Arc0, the chains segregate about 80% of the cases. However, we checked that shorter ring polymers with 100 monomers can easily segregate even without effects of topoisomerase, as seen previously [17]. The values of τ_S for different architectures is given Fig.2c; τ_s is calculated by averaging over the runs that lead to successful chromosome segregation, from a pool of 10 independent runs. Thus the quicker segregation with the Arc-2 polymer is a consequence of the enhanced entropic repulsion between the two daughter DNAs due to the presence of internal loops in each ring-polymer. We show that each loop-COM gets separated along the cylinder-axis once the loops get created by CLs, refer SI-IV Fig.S3. Furthermore if we have an architecture with two additional

CLs over and above the CLs in Arc-2 architecture, i.e. the Arc-2-2 architecture with 4 loops (discussed in detail later), then they segregate even faster.

At the first step of the replication process of our model, a new *oriC* monomer is created and is named the *oriC* of the D2-chain. Hence we see in Fig.2d, that the two (replicated) *oriC*s start off from the middle of the cylinder. The two additional CLs are created after 2.5×10^7 MCS. Once the CLs are introduced between the newly added 125-th and the 375-th monomer and *oriC* of the D2-chain, we see sharp change in *oriC* position of the D2-polymer chain (bottom red line). For the monomers on the other chain, we only change the monomer status from mother to daughter as RF position moves along the contour and rename it monomers of DNA-1, and hence the CL between *oriC*-125 and *oriC*-375 monomers existed from the start of replication. After the loops of D2 are created, we observe that the *oriC* starts migrating out to occupy the 1/4 and 3/4 positions (scaled by the final length of the cylinder L_f) on the elongated cylinder axis.

In Fig.3(a,b) we follow the positions of the monomers corresponding to loci labelled as *oriC*, R1, R2, R3, L1, L2 and *dif-ter* [23], as function of MCS. We see that different loci segregate out to two different halves of the cylinder after replication; data is plotted from the stage

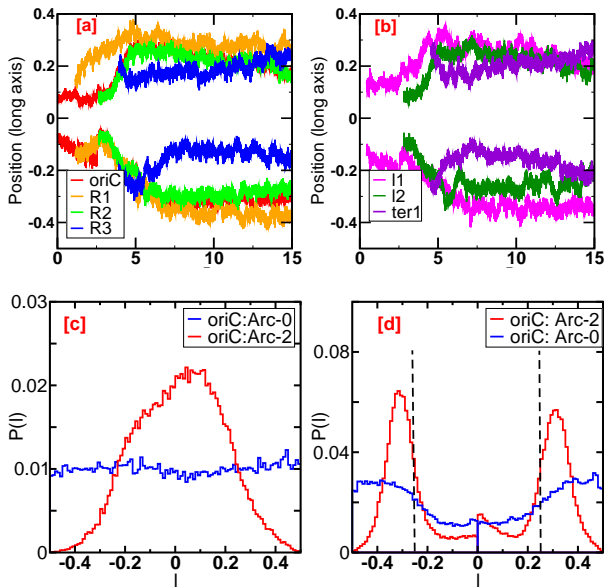


FIG. 3. The data shows the trajectory of the (a) *oriC* R1, R2 and R3 loci and (b) L1, L2, and *ter1* loci after the replication of the locus, along the cylinder long axis for loop architecture 2 and $\kappa_{cl} = 100k_B T/a^2$. To plot the locus trajectories we average over 20 independent runs and scale it by the final length of the confining cylinder. We follow the conventions of the 'polar orientation' as in [23], where the replicated locus is assigned the negative axis. (c) Probability distribution of the *oriC* position before replication, for Arc-0 and Arc-2. We note that Arc2 shows a narrow distribution around the mid-cell while for Arc-0 *oriC* shows a uniform distribution. (d) Probability distribution of the *oriC* position post replication, for Arc-0 and Arc-2. Data is collected from 20 independent runs from $10 - 15 \times 10^7$ MCS. The black dashed lines represent the quarter positions and have been incorporated for aid of visualization. We note that Arc-2 shows a narrower distribution approximately around the quarter positions, as compared to Arc-0.

that the RFs reach the individual monomer locus, and is replicated. We observe that though the *oriC* is replicated at the beginning of the simulation, it branches out to two halves of the cylinder only after the loops in D2 chain are created. This matches with the observation of cohesion time in experiments. Other than *oriC* and R1, other loci have extremely low cohesion times. Data shown is averaged over 20 independent runs, starting from statistically independent initial conditions.

The mutual repulsion between internal loops in an (unreplicated) DNA-polymer with Arc-2 architecture also localizes the *oriC* to the middle of the cylinder at the beginning of replication process. We create an equilibrium structure of a single Arc-2 DNA-polymer to simulate an unreplicated chromosome and we observe that the *oriC* localizes to the middle of the cylinder with $L_i = 17.5a$ which is as seen in-vivo: refer Fig.3c. In contrast, the *oriC* of a ring polymer with 500 monomers (Arc-0) is found non-localized along the cylinder axis under equilibrium conditions. Subsequently, if replication is switched

on, the *oriC*s move to the two quarter positions along the cell axis for the (daughter) DNA-polymers with Arc-2, as shown in Fig.2d.

In Fig.3d, we plot the probability distribution $P(l)$ of finding the two *oriC*s of DNA-1 and DNA-2, and show the distribution is sharply peaked around the quarter positions for Arc-2 architecture as compared to the two *oriC*s daughter-polymers with Arc-0 architecture. Similar data for the other loci is given in SI-V and in Fig.S4. Thus the presence of loops localizes all the different loci in complete agreement with experiments reported in [23]. As we see in Fig.3a,b all loci reach their home positions after segregation by the end of 8×10^7 MCS. But we start collecting statistical data to plot the distributions in Fig.3d after 10×10^7 MCS from the start of simulation. Thus each loci reaches its home position before we collect statistical data for the next 5×10^7 MCS to calculate $P(l)$. We do not model the division of the cell, hence each locus continues to fluctuate around its home position till 15×10^7 MCS. We can unambiguously conclude from the width of each distribution that each loci is localized at their home positions, and the two *oriC*s, specifically are at the quarter and three-quarters positions, respectively.

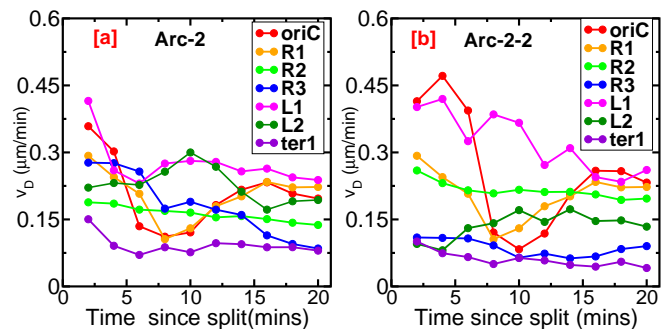


FIG. 4. Figure shows the drift velocity v_D for individual loci as a function of time (converted from MCS) obtained with (a) Arc-2 and (b) Arc-2-2. Completion of replication takes 5×10^7 iterations or 33 mins for both cases. Details of methodology for calculating v_D is outlined in the SI-VI. The drift velocity of loci show universal behavior, i.e, values of v_D are quite similar close to the onset of segregation, as well as later times, as shown in-vivo [23]. Conversion from MCS to time units enables easy comparison with experiments [23].

To quantitatively establish that we indeed reproduce the dynamics of loci-segregation as seen in-vivo by [23], we measure the drift velocity of segregation of the individual loci. The procedure for measuring the drift velocity is outlined in SI, section VI. We show that we reproduce some aspects of the universal behavior, in that they have similar values of local velocities 5 minutes after the onset of segregation of loci. We have not looked at smaller time intervals as in [23], because of the difficulty in getting good statistical averages for the value of the speed of certain loci. But more strikingly, we reproduce similar values of drift velocity (within the acceptable range of fluctuations), as seen in Fig.7 of [23],

at similar times after the replication of reference loci. However, in [23] the *oriC* locus shows a higher drift velocity than other loci at long times, viz. after 15 minutes after replication. A more detailed and accurate model might reproduce this aspect, but we would like to keep our model as simple and minimalist as possible.

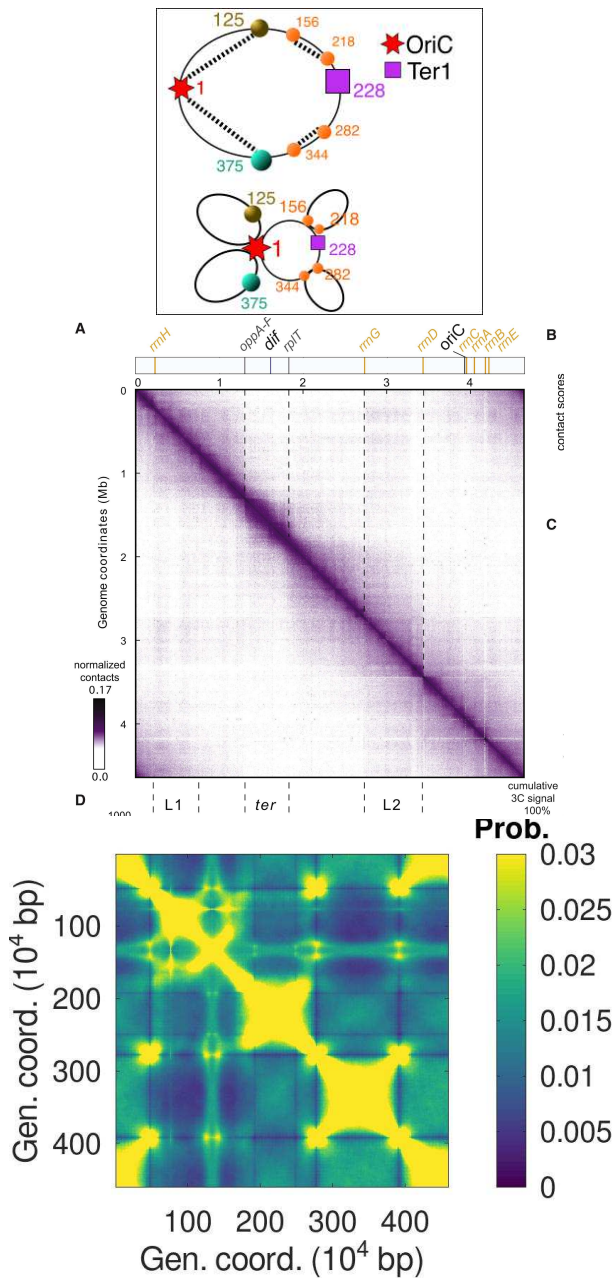


FIG. 5. (a) Schematic showing the cross-linking sites in Arc-2-2 architecture. (b) shows the experimental contact map for *E. coli* chromosomes as published in [25]. The figure is being shown for aid of comparison with the simulated contact map, after obtaining requisite permissions. (c) shows the contact map obtained from simulations with Arc-2-2 architecture, averaged over 10 independent runs.

Having quantitatively matched several experimental

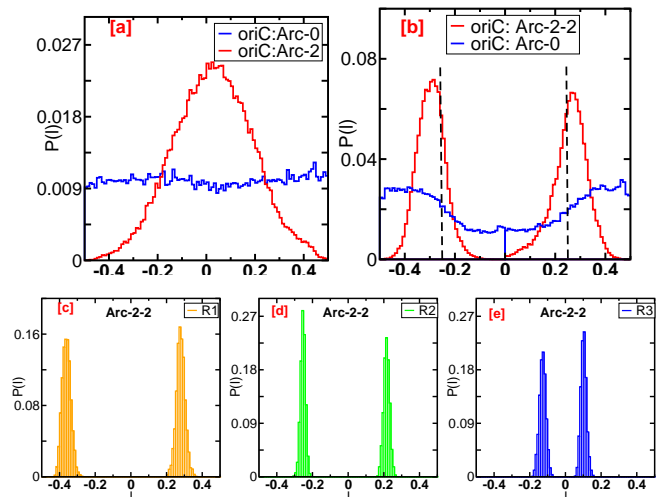


FIG. 6. (a) Probability distribution of the *oriC* position before replication, for Arc0 and Arc-2-2, averaged over 10 independent runs. We note that Arc-2-2 shows a narrow distribution around the midcell while for Arc0 *oriC* shows a uniform distribution. (b) Probability distribution of the *oriC* position post replication, for Arc0 and Arc-2-2. Data is collected from 20 independent runs from 5×10^7 MCS to 15×10^7 minutes. The black dashed lines represent the quarter positions and have been incorporated for aid of visualization. We note that Arc-2-2 shows a narrower distribution approximately around the quarter positions, as compared to Arc0. Probability distribution of the (c) R1, (d) R2 and (e) R3 locus post replication for Arc-2-2. The probability distributions in (c), (d) and (e) have been calculated from the averaged trajectory curves (given in S.I-VIII and Fig.S6), from a simulation time of 5×10^7 MCS to 15×10^7 MCS.

results related to spatio-temporal dynamics of DNA loci in the B, C period of *E. coli* cell cycle using the Arc-2 architecture, we wish to examine whether our modified polymer architecture is able to reproduce certain traits of the Hi-C contact maps [25]. The Hi-C data is obtained for a large ensemble of cells, each of which is at a different stage in its cell cycle. To that end we show a simulated contact map using data for the coordinates of different monomers over the entire life cycle i.e. upto 8×10^7 MCS plotted in genomic coordinates, with our architecture. we give more details of how we collect data for Contact maps in the SI-VII. We note that Arc-2 fails to reproduce the experimental contact map (refer Si-VII, Fig.S5). However a slight modification of our polymer architecture by adding two additional CLs, with links between monomer number 156 and 218 on one arm and 344 and 282 on the other arm, lead to the Arc-2-2 architecture. This results in a contact map that has 4 bright domains roughly of size 1Mbp each refer Fig.5.

The first macro-domain (L1) extends from 0.2 – 1.2 Mbp, the second (*ter* macrodomain) from approximately 1.2 – 1.8 Mbp and the third (L2) from 2.8 – 3.5 Mbp. Thus we note that the positions of our macrodomains are in fair agreement with the experimentally determined

contact map given in Fig.5b, which has been reproduced from [25]. Thus a slight modification of our chosen polymer architecture also leads to the formation of macro-domains as seen in-vivo. Moreover, the Arc-2-2 leads to lower segregation times τ_S as compared to Arc-2 (Fig.2c), and also localizes the *oriC* and other loci even better than the Arc-2 architecture with very similar migration dynamics : refer data presented in Fig.6 and SI-IX, Fig.S7 in the Supplementary.

To show that the obtained results are robust, we validate our results for similar simulation studies but with 1000 monomers, where each bead represents 4.6 kbp of DNA (refer SI-X and Fig.S8 in the Supplementary). Furthermore, in order to understand whether our hypothesised polymer architectures can shed light on seemingly contrarian points of view, about the spatial positions of the replication forks, we plot the trajectory of the replication forks for Arc-2 and Arc-2-2 architectures. We find that the trajectory shows an 'M' like pattern, which is directly indicative of the underlying polymer architecture (refer SI-XI and Fig.S9). Thus the replication forks are located close to the mid-cell position both at the beginning and the end of the replication process. It is plausible in our opinion, that a detailed study of the underlying polymer architecture may thus resolve the differences in the "Train track model" and the "Replication factory" models of replication.

I. DISCUSSION

Thus we conclude that a modification of the polymer architecture by adding 4 loops (or 2 loops) to the ring-polymer to form the Arc-2-2 architecture (or Arc-2 architecture) is favourable for *E. coli* DNA-polymer efficient segregation during replication. We hypothesize that such "effective" cross-links across large genomic distances may arise due to the presence of MukBeF (or other SMCs) which are known to bridge distant chromosomal regions. The observation of macro-domains in contact maps and the similarity in the values of drift velocity observed for all loci emerge organically as a consequence of the adopting the Arc-2-2 architecture. The reason for the localization of the two *oriCs* (to the quarter positions), and other loci is the entropic repulsion between the loops within each individual daughter chromosome. The loops belonging to the same daughter try to occupy different positions within the two halves of the cylinder.

Our study also reconciles observations from the train track model and replication factory models regarding the location of the replication fork. Initially the replication begins at the cell-center as the *oriC* of the unreplicated chromosome is localized there. Then the site of replication migrate out from the cell center as daughter polymer architecture gets modified to Arc-2 or Arc-2-2. But finally replication ends near the cell center as *dif-ter* locus gets localized at cell center midway through the replication. In an earlier simulation study [12], the unreplicated

DNA polymer was forcibly constrained within a smaller cylinder within a concentric shell arrangement. However, we did not have to use the concentric shell model of [12], as compaction of the mother DNA-polymer was achieved to some degree, by the Arc-2-2 (or Arc-2) architecture of the unreplicated chromosome at the beginning of replication.

Monte Carlo was the simulation technique of choice as we primarily relied on diffusive dynamics to achieve entropic segregation. It also enabled us to (a) introduce springs to model CLs, (b) change the diameter of the monomers at regular intervals to allow chain crossing and (c) also have fast and many independent runs (as compared to Molecular dynamics). The frequency with which we change monomer diameter to allow for chain crossing is important to achieve successful segregation. If we reduce diameter too frequently or have small diameters for prolonged periods, entropic forces arising from excluded volume interactions will be suppressed. On the other hand, we checked that if the release of topological constraints is too infrequent, that again leads to inefficient segregation. We also varied replication rates, viz., we introduce monomers at rates either faster or slower than the rates reported in this manuscript. A choice significantly different from this rate leads inefficient segregation. We have a mapping of time scales which enables us to introduce monomers every 2×10^5 MCS which is very close to experimentally known rates. This mapping relies on the monomer size being ≈ 150 nm incorporating compaction effects at lower length scales. We report consequences of choice of different replication rates, as well as calculations of free energy differences for systems of polymers (with different architectures) in mixed state versus in segregated state in future communications, along with data for fast growth.

While the match of the calculated contact map with the experimental map is an consequence of the presence of the long-lived links between very specific monomers, our prediction of the location of CLs along the chain contour can now be explicitly verified. We had checked that change in position of CLs by 4-5 monomers on either side of the chain contour does not significantly alter results. However, how the SMC proteins bridges different DNA-segments well separated in space within the cylindrical cell has remained an open question and remains so [32]. Furthermore it is quite plausible that the process of "cross-linking" which we have implemented in the simulations, might be realised by distant genomic segments diffusing closer to each other. Thus it is possible that the "effective crosslinks" proposed herein, is achieved in reality over longer timescales than those implemented here. Future experimental studies may shed light on this aspect. Moreover, the cell is quite packed with organelles which act as crowders, which could affect segregation dynamics and organization [60, 61]. Thus more detailed studies incorporating these aspects may prove to be particularly useful.

II. ACKNOWLEDGEMENTS

A.C., with DST-SERB identification SQUID-1973-AC-4067, acknowledges funding by DST-India, project

MTR/2019/000078 and discussions in meetings organized by ICTS, Bangalore, India. A.C. thanks Suckjoon Jun for drawing our attention to some unresolved aspects pertaining to bacterial chromosome segregation for fast growth conditions back in 2018.

-
- [1] Rob Phillips, Jane Kondev, Julie Theriot, Hernan G. Garcia, and Nigel Orme. *Physical Biology of the Cell*. Garland Science, October 2012.
- [2] Andrei Kuzminov. The chromosome cycle of prokaryotes. *Molecular Microbiology*, 90(2):214–227, 2013.
- [3] Jay K. Fisher, Aude Bourniquel, Guillaume Witz, Beth Weiner, Mara Prentiss, and Nancy Kleckner. Four-dimensional imaging of *e. coli* nucleoid organization and dynamics in living cells. *Cell*, 153(4):882–895, 2013.
- [4] Liselot Dewachter, Natalie Verstraeten, Maarten Fauvart, and Jan Michiels. An integrative view of cell cycle control in *escherichia coli*. *FEMS Microbiology Reviews*, 42(2):116–136, January 2018.
- [5] Aleksandre Japaridze, Christos Gogou, Jacob W. J. Kerssemakers, Huyen My Nguyen, and Cees Dekker. Direct observation of independently moving replisomes in *escherichia coli*. *Nature Communications*, 11(1), June 2020.
- [6] Jarno Mäkelä and David J. Sherratt. Organization of the *escherichia coli* chromosome by a MukBEF axial core. *Molecular Cell*, 78(2):250–260.e5, April 2020.
- [7] Sarah M. Mangiameli, Julie A. Cass, Houra Merrikh, and Paul A. Wiggins. The bacterial replisome has factory-like localization. *Current Genetics*, 64(5):1029–1036, April 2018.
- [8] Anjana Badrinarayanan, Tung B.K. Le, and Michael T. Laub. Bacterial chromosome organization and segregation. *Annual Review of Cell and Developmental Biology*, 31(1):171–199, November 2015.
- [9] S. Ben-Yehuda. RacA, a bacterial protein that anchors chromosomes to the cell poles. *Science*, 299(5606):532–536, December 2002.
- [10] Mark A. Umbarger, Esteban Toro, Matthew A. Wright, Gregory J. Porreca, Davide Baù, Sun-Hae Hong, Michael J. Fero, Lihua J. Zhu, Marc A. Marti-Renom, Harley H. McAdams, Lucy Shapiro, Job Dekker, and George M. Church. The three-dimensional architecture of a bacterial genome and its alteration by genetic perturbation. *Molecular Cell*, 44(2):252–264, October 2011.
- [11] Grant R. Bowman, Luis R. Comolli, Jian Zhu, Michael Eckart, Marcelle Koenig, Kenneth H. Downing, W.E. Moerner, Thomas Earnest, and Lucy Shapiro. A polymeric protein anchors the chromosomal origin/ParB complex at a bacterial cell pole. *Cell*, 134(6):945–955, September 2008.
- [12] S. Jun and B. Mulder. Entropy-driven spatial organization of highly confined polymers: Lessons for the bacterial chromosome. *Proceedings of the National Academy of Sciences*, 103(33):12388–12393, August 2006.
- [13] Suckjoon Jun and Andrew Wright. Entropy as the driver of chromosome segregation. *Nature Reviews Microbiology*, 8(8):600–607, August 2010.
- [14] Fabai Wu, Pinaki Swain, Louis Kuijpers, Xuan Zheng, Kevin Felter, Margot Guurink, Jacopo Solari, Suckjoon Jun, Thomas S. Shimizu, Debasish Chaudhuri, Bela Mulder, and Cees Dekker. Cell boundary confinement sets the size and position of the *e. coli* chromosome. *Current Biology*, 29(13):2131–2144.e4, July 2019.
- [15] J. Pelletier, K. Halvorsen, B.-Y. Ha, R. Paparccone, S. J. Sandler, C. L. Woldringh, W. P. Wong, and S. Jun. Physical manipulation of the *escherichia coli* chromosome reveals its soft nature. *Proceedings of the National Academy of Sciences*, 109(40):E2649–E2656, September 2012.
- [16] Suckjoon Jun, Axel Arnold, and Bae-Yeun Ha. Confined space and effective interactions of multiple self-avoiding chains. *Physical Review Letters*, 98(12), March 2007.
- [17] Youngkyun Jung, Suckjoon Jun, and Bae-Yeun Ha. Self-avoiding polymer trapped inside a cylindrical pore: Flory free energy and unexpected dynamics. *Physical Review E*, 79(6), June 2009.
- [18] Axel Arnold and Suckjoon Jun. Time scale of entropic segregation of flexible polymers in confinement: Implications for chromosome segregation in filamentous bacteria. *Physical Review E*, 76(3), September 2007.
- [19] C. Helmstetter, S. Cooper, O. Pierucci, and E. Revelas. On the bacterial life sequence. *Cold Spring Harbor Symposia on Quantitative Biology*, 33(0):809–822, January 1968.
- [20] W. D. DONACHIE. Relationship between cell size and time of initiation of DNA replication. *Nature*, 219(5158):1077–1079, September 1968.
- [21] Arieh Zaritsky, Waldemar Vollmer, Jaan Männik, and Chenli Liu. Does the nucleoid determine cell dimensions in *escherichia coli*? *Frontiers in Microbiology*, 10, August 2019.
- [22] B. Youngren, H. J. Nielsen, S. Jun, and S. Austin. The multifork *escherichia coli* chromosome is a self-duplicating and self-segregating thermodynamic ring polymer. *Genes & Development*, 28(1):71–84, January 2014.
- [23] Julie A. Cass, Nathan J. Kuwada, Beth Traxler, and Paul A. Wiggins. *Escherichia coli* chromosomal loci segregate from midcell with universal dynamics. *Biophysical Journal*, 110(12):2597–2609, 2016.
- [24] Andreas Hofmann, Jarno Mäkelä, David J Sherratt, Dieter Heermann, and Seán M Murray. Self-organised segregation of bacterial chromosomal origins. *eLife*, 8, August 2019.
- [25] Virginia S. Liroy, Axel Cournac, Martial Marbouty, Stéphane Duigou, Julien Mozziconacci, Olivier Espéli, Frédéric Boccard, and Romain Koszul. Multiscale structuring of the *e. coli* chromosome by nucleoid-associated and condensin proteins. *Cell*, 172(4):771–783.e18, February 2018.
- [26] Tung BK Le and Michael T Laub. New approaches to understanding the spatial organization of bacterial genomes. *Current Opinion in Microbiology*, 22:15–21, December 2014.

- [27] T. B. K. Le, M. V. Imakaev, L. A. Mirny, and M. T. Laub. High-resolution mapping of the spatial organization of a bacterial chromosome. *Science*, 342(6159):731–734, October 2013.
- [28] Mark A. Umbarger, Esteban Toro, Matthew A. Wright, Gregory J. Porreca, Davide Baù, Sun-Hae Hong, Michael J. Fero, Lihua J. Zhu, Marc A. Marti-Renom, Harley H. McAdams, Lucy Shapiro, Job Dekker, and George M. Church. The three-dimensional architecture of a bacterial genome and its alteration by genetic perturbation. *Molecular Cell*, 44(2):252–264, October 2011.
- [29] Hironori Niki, Yoshiharu Yamaichi, and Sota Hiraga. Dynamic organization of chromosomal dna in escherichia coli. *Genes & Development*, 274(3):212–223, August 1998.
- [30] Michèle Valens, Stéphanie Penaud, Michèle Rossignol, François Cornet, and Frédéric Boccard. Macrodome organization of the escherichia coli chromosome. *The EMBO Journal*, 23(21):4330–4341, October 2004.
- [31] Ivan Junier, Frédéric Boccard, and Olivier Espéli. Polymer modeling of the E. coli genome reveals the involvement of locus positioning and macrodomain structuring for the control of chromosome conformation and segregation. *Nucleic Acids Research*, 42(3):1461–1473, 11 2013.
- [32] Virginia S. Liroy, Ivan Junier, and Frédéric Boccard. Multiscale dynamic structuring of bacterial chromosomes. *Annual Review of Microbiology*, 75(1), August 2021.
- [33] Edward J Banigan, Aafke A van den Berg, Hugo B Brandão, John F Marko, and Leonid A Mirny. Chromosome organization by one-sided and two-sided loop extrusion. *eLife*, 9, April 2020.
- [34] Andrea M. Chiariello, Carlo Annunziatella, Simona Bianco, Andrea Esposito, and Mario Nicodemi. Polymer physics of chromosome large-scale 3d organisation. *Scientific Reports*, 6(1), July 2016.
- [35] Tejal Agarwal, G P Manjunath, Farhat Habib, Pavana Lakshmi Vaddavalli, and Apratim Chatterji. Role of special cross-links in structure formation of bacterial DNA polymer. *Journal of Physics: Condensed Matter*, 30(3):034003, December 2017.
- [36] Abdul Wasim, Ankit Gupta, and Jagannath Mondal. Mapping the multiscale organisation of escherichia coli chromosome in a hi-c-integrated model. June 2020.
- [37] Geoffrey Fudenberg, Maxim Imakaev, Carolyn Lu, Anton Goloborodko, Nezar Abdennur, and Leonid A. Mirny. Formation of chromosomal domains by loop extrusion. *Cell Reports*, 15(9):2038–2049, May 2016.
- [38] Tejal Agarwal, G. P. Manjunath, Farhat Habib, and Apratim Chatterji. Origin of spatial organization of DNA-polymer in bacterial chromosomes. *EPL (Europhysics Letters)*, 121(1):18004, January 2018.
- [39] Tejal Agarwal, G. P. Manjunath, Farhat Habib, and Apratim Chatterji. Bacterial chromosome organization. i. crucial role of release of topological constraints and molecular crowders. *The Journal of Chemical Physics*, 150(14):144908, April 2019.
- [40] Tejal Agarwal, G. P. Manjunath, Farhat Habib, and Apratim Chatterji. Bacterial chromosome organization. II. few special cross-links, cell confinement, and molecular crowders play the pivotal roles. *The Journal of Chemical Physics*, 150(14):144909, April 2019.
- [41] Remus T. Dame, Fatema-Zahra M. Rashid, and David C. Grainger. Chromosome organization in bacteria: mechanistic insights into genome structure and function. *Nature Reviews Genetics*, 21(4):227–242, November 2019.
- [42] Fabai Wu, Pinaki Swain, Louis Kuijpers, Xuan Zheng, Kevin Felter, Margot Guurink, Jacopo Solari, Suckjoon Jun, Thomas S. Shimizu, Debasish Chaudhuri, Bela Mulder, and Cees Dekker. Cell boundary confinement sets the size and position of the e. coli chromosome. *Current Biology*, 29(13):2131–2144.e4, July 2019.
- [43] Henrik J. Nielsen, Brenda Youngren, Flemming G. Hansen, and Stuart Austin. Dynamics of escherichia coli chromosome segregation during multifork replication. *Journal of Bacteriology*, 189(23):8660–8666, December 2007.
- [44] Mario Nicodemi and Ana Pombo. Models of chromosome structure. *Current Opinion in Cell Biology*, 28:90–95, June 2014.
- [45] Peter R Cook and Davide Marenduzzo. Transcription-driven genome organization: a model for chromosome structure and the regulation of gene expression tested through simulations. *Nucleic Acids Research*, 46(19):9895–9906, September 2018.
- [46] Ajoy Maji, Jahir A. Ahmed, Subhankar Roy, Buddhapriya Chakrabarti, and Mithun K. Mitra. A lamin-associated chromatin model for chromosome organization. *Biophysical Journal*, 118(12):3041–3050, June 2020.
- [47] Ajoy Maji, Ranjith Padinhateeri, and Mithun K. Mitra. The accidental ally: Nucleosome barriers can accelerate cohesin-mediated loop formation in chromatin. *Biophysical Journal*, 119(11):2316–2325, December 2020.
- [48] Ankit Agrawal, Nirmalendu Ganai, Surajit Sengupta, and Gautam I. Menon. Nonequilibrium biophysical processes influence the large-scale architecture of the cell nucleus. *Biophysical Journal*, 118(9):2229–2244, May 2020.
- [49] Nick Gilbert and Davide Marenduzzo. Genome organization: experiments and modeling. *Chromosome Research*, 25(1):1–4, February 2017.
- [50] Ivan Junier, Olivier Martin, and François Képès. Spatial and topological organization of DNA chains induced by gene co-localization. *PLoS Computational Biology*, 6(2):e1000678, February 2010.
- [51] Johan H. Gibcus, Kumiko Samejima, Anton Goloborodko, Itaru Samejima, Natalia Naumova, Johannes Nuebler, Masato T. Kanemaki, Linfeng Xie, James R. Paulson, William C. Earnshaw, Leonid A. Mirny, and Job Dekker. A pathway for mitotic chromosome formation. *Science*, 359(6376):eaao6135, January 2018.
- [52] Debasish Chaudhuri and Bela M. Mulder. Spontaneous helicity of a polymer with side loops confined to a cylinder. *Physical Review Letters*, 108(26), June 2012.
- [53] Pinaki Swain, Bela M. Mulder, and Debasish Chaudhuri. Confinement and crowding control the morphology and dynamics of a model bacterial chromosome. *Soft Matter*, 15(12):2677–2687, 2019.
- [54] Thomas J. Lampo, Nathan J. Kuwada, Paul A. Wiggins, and Andrew J. Spakowitz. Physical modeling of chromosome segregation in escherichia coli reveals impact of force and DNA relaxation. *Biophysical Journal*, 108(1):146–153, January 2015.
- [55] Olivier Espéli and Frédéric Boccard. Organization of the escherichia coli chromosome into macrodomains and its possible functional implications. *Journal of Structural Biology*, 156(2):304–310, November 2006.
- [56] Nancy Kleckner, Jay K Fisher, Mathieu Stouf, Martin A White, David Bates, and Guillaume Witz. The bacte-

- rial nucleoid: nature, dynamics and sister segregation. *Current Opinion in Microbiology*, 22:127–137, December 2014.
- [57] Frank Uhlmann. SMC complexes: from DNA to chromosomes. *Nature Reviews Molecular Cell Biology*, 17(7):399–412, April 2016.
- [58] L. Postow. Topological domain structure of the *Escherichia coli* chromosome. *Genes & Development*, 18(14):1766–1779, July 2004.
- [59] Jarno Mäkelä, Stephan Uphoff, and David J. Sherratt. Nonrandom segregation of sister chromosomes by *Escherichia coli* MukBEF. *Proceedings of the National Academy of Sciences*, 118(33):e2022078118, August 2021.
- [60] Marc Joyeux. Compaction of bacterial genomic DNA: clarifying the concepts. *Journal of Physics: Condensed Matter*, 27(38):383001, September 2015.
- [61] Marc Joyeux. A segregative phase separation scenario of the formation of the bacterial nucleoid. *Soft Matter*, 14(36):7368–7381, 2018.